RECENT RESULTS FROM THE MARS GLOBAL SURVEYOR Ka-BAND LINK EXPERIMENT (MGS/KABLE-II)

D. Morabito, S. Butman, and S. Shambayati
Jet Propulsion Laboratory, California Institute of Technology
D. Morabito M/S 161-260, 4800 Oak Grove Drive, Pasadena, California, 91109, USA
Phone: 818-354-2424; Fax: 818-393-4643; E-mail: ddm@rodan.jpl.nasa.gov

ABSTRACT

The Mars Global Surveyor (MGS) spacecraft, launched on November 7, 1996, carries an experimental space-to-ground telecommunications link at Ka-band (32 GHz) along with the primary X-band (8.4 GHz) downlink. The signals are simultaneously transmitted from a 1.5-m diameter parabolic antenna on MGS and received by a beam-waveguide R&D 34-meter antenna located in NASA's Goldstone Deep Space Network (DSN) complex near Barstow, California. This Ka-band link experiment allows the performances of the Ka-band and X-band signals to be compared under nearly identical conditions. The two signals have been regularly tracked during the past two years. This article presents carrier signal level data (Pc/No) for both X-band and Ka-band acquired over a wide range of station elevation angles, weather conditions, and solar elongation angles. The cruise period covers the period from launch (November 7, 1996) to Mars orbit capture (September 12, 1997). Since September 12, 1997, MGS has been in orbit around Mars. These measurements reconfirm that Ka-band could increase data capacity by at least a factor of three (5 dB) compared to X-band. During May 1998, the solar corona experiment was conducted in which the effects of solar plasma on the X-band and Ka-band links were studied. In addition, difference (f_x-f_{Ka}/3.8) frequency data results will be presented.

The MGS/KaBLE-II link experiment measured signal strengths which were in general agreement with predicted values, and frequency residuals which were in agreement between bands and whose statistics were consistent with expected noise sources. The relative performance of X and Ka-band over an extended period will continue to be quantified as additional data are acquired under a wide range of elevation angles and atmospheric conditions. These efforts will continue with MGS/KaBLE-II as well as a future spacecraft with Ka-band and X-band signals, DS-1, which is scheduled for launch in October 1998.

1. INTRODUCTION

The capability to communicate across interplanetary distances has grown by several orders of magnitude since the advent of space exploration about 40 years ago. A shift to Ka-Band (32 GHz) is projected to add 6 dB of improvement over X-band band (8.4 GHz), the primary downlink frequency today. The increase in antenna gain with Ka-band is theoretically 11.6 dB relative to X-band, however, atmospheric noise and attenuation diminishes that by 4 to 5 dB. A further loss of 1.5 to 2 dB is due to DSN antenna imperfections that are less significant at X-band. In terms of spacecraft mass and power savings, the anticipated 6 dB improvement requires Ka-band transmitters that are no more massive nor less efficient than those at X-band.

To determine if Ka-band will be viable operationally requires performance data to be gathered under varying operating conditions; with weather, DSN antenna elevation, solar elongation angle, and spacecraft modes over a statistically significant period. This is accomplished by MGS/KaBLE which broadcasts simultaneously in both frequency bands. The MGS/KaBLE equipment has been functioning well. Signal level and frequency data have been acquired from 189 observing tracks conducted over the past two years since launch, and these data will be described in this paper. End-to-end telemetry and ranging demonstrations were successfully conducted and the results presented last year (Butman et. al. 1997). MGS is pointing within 0.1° and the DSS 13 antenna tracking error is less than 1 mdeg. The signals from MGS have also been tracked through the Solar Conjunction period of May 1998 in order to observe propagation effects through the solar plasma. MGS/KaBLE has also been used to check out DSS 25, the new 34 m station currently being prepared to

support the X-band and Ka-band downlinks on the Cassini and DS-1 missions. This paper briefly describes the spacecraft and ground systems and presents updated results from those reported last year.

2. SPACECRAFT CONFIGURATION

The MGS mission was conceived as a low-cost, rapid replacement for Mars Observer (MO) which was lost on August 18, 1993. MO carried the original KaBLE which functioned well given its limitations (Rebold et. al. 1994). The MGS spacecraft includes a functional equivalent of MO/KaBLE which incorporates added requirements of increased Ka-band EIRP and transmitting within the allocated 31.8-32.3 GHz deep-space frequency band. The KaBLE hardware is described in detail by Butman et. al. 1997.

3. GROUND SYSTEM CONFIGURATION

The DSS 13 ground station configuration for KaBLE-II will be described here. On the beam-waveguide antenna, the mirrors guide and focus the RF energy onto a feed horn and to a low noise amplifier (LNA). A dichroic plate enables simultaneous reception of both X-band and Ka-band signals. The Ka-band monopulse receiver enables the antenna to autotrack on the spacecraft signal to 1 mdeg accuracy. The Ka-band antenna efficiency varies from 30% to 57% depending upon elevation angle and feed position. The system operating noise temperature (Top) as measured by the total power radiometer (TPR) is elevation dependent and changes with weather.

3a) Monopulse Feed-LNA Package

All of the MGS KaBLE-II experiments after January 1997 at DSS-13 used the monopulse feed package to acquire the Ka-band data. The initial first few experiments between December 1996 and January 1997 used the Array Feed Ka-band package to acquire Ka-band data. The monopulse receiver system is used to actively correct antenna pointing using the received Ka-band signal levels.

During experiments, the antenna is initially pointed using spacecraft pointing predicts. The monopulse computer determines the pointing error and the corrects for the mis-pointing by sending elevation and cross-elevation offsets to the antenna pointing computer every few seconds. For the majority of the passes conducted using the monopulse tracking system, the average pointing errors were less than 1 mdeg. During high gusty wind conditions, the errors were less than 2 mdeg. For some passes in which the monopulse receiver was not tracking, manual pointing offsets were performed to peak onto the Ka-band signal.

During the period from 97-160 to 97-205, a degradation in Ka-band signal level was observed and eventually traced to ice which was discovered inside the monopulse feedhorn window. This ice caused the monopulse tracking system to incorrectly peak onto the spacecraft signal. Shortly after the ice was discovered, the monopulse package was warmed-up and cooled back down on 97-206 in order to get rid of the accumulated ice. The cracked feedhorn window assembly was replaced shortly afterwards on day 97-216.

3b) Experimental Tone Tracker (ETT)

The Experimental Tone Tracker (ETT) is a digital phase-lock-loop (PLL) receiver which was used to simultaneous track both X-band and Ka-band carrier signals during the MGS KaBLE-II tracks at DSS-13. The ETT has been very reliable, operating virtually without failure. A very useful feature of the ETT is that when locked to a strong signal it can be set to aid a weak coherent signal. Once a signal is detected, the ETT processing utilizes a PLL which produces an estimate of the SNR (Pc/No) in a 1-Hz bandwidth as well as phase and frequency. The ETT estimates of very precise phase at 1-second time samples are converted to very accurate frequency estimates by the KaBLE analysis software.

3c) Telemetry Processing Equipment

Two digital receiver-processors, TP-2 and TP-13, have been used to receive and demodulate the X and Ka-band downlinks. TP-13 is dedicated to the X-band channel, TP-2 to the Ka-band channel. The receivers have been used to acquire and track carrier, subcarrier and symbols. The measured carrier and data channel signal levels have been used to derive accurate modulation indices which were used to compute carrier suppression corrections for predicted Pc/No signal levels discussed in Section 4. A successful demonstration of

processing the telemetry data on the Ka-band link using operational DSN equipment was previously presented (Butman et. al. 1997).

3d) Total Power Radiometer (TPR)

The Total Power Radiometer (TPR) measures received signal and noise using 10 to 30 MHz filters. The TPR data are used to provide the thermal noise (No) estimates to the Pc/No predictions. When the antenna is pointed a few degrees away from the spacecraft, the TPR measures only the system noise. Radiometer calibrations are routinely conducted prior to every KaBLE track using ambient loads. However, on 97-318 it was discovered that the Ka-band ambient load was improperly configured since the monopulse package was installed in January 1997. The problem was then corrected. For passes conducted between 97-035 and 97-318, radiometer data acquired using a noise diode were used to calibrate system gain.

3e) Ancillary Data

In addition to the above, ancillary water vapor radiometry (WVR) data and surface meteorological data are also acquired for use in the estimation of weather effects, and attenuation in the Pc/No predicts.

4. RESULTS

This section will describe results on X-band and Ka-band signal strength data acquired during cruise and Mars orbit from December 1996 to May 1998 (4a), signal strength data acquired during MGS solar conjunction in May 1998 (4b), and dual-band frequency data acquired between January 1997 to May 1998 (4c).

4a) Signal Strengths.

A total of 189 tracking passes were conducted between December 1996 and May 1998. In the majority of the passes, a Ka-band signal was detected, locked onto and tracked for a significant duration of each track. The received signal strengths vary due to spacecraft range, pointing, modulation index, ranging modulation, ground station configuration, weather attenuation, uncertainties in pointing, KaBLE flight temperature and downlink frequency. During the 144 passes for which Ka-band signals were tracked with minimum ground station pointing loss, the atmospheric attenuation averaged over a pass varied from 0.1 to 0.9 dB.

Most data at DSS-13 were acquired by tracking the residual carrier with the ETT, and with the spacecraft configured on the HGA. Figure 1 is an example of X-band and Ka-band carrier (Pc/No) data acquired during a clear weather pass conducted on 97-212. Figure 2 displays the concurrent Top data recorded at Ka-band for this pass. Figure 3 is an example of Pc/No data acquired during a cloudy and rainy weather pass on 97-203. Figure 4 displays the Ka-band Top data recorded at Ka-band for pass 97-203. Note that the signal level variations in the Ka-band Pc/No in Figure 3 are clearly negatively-correlated with the Ka-band Top variations in Figure 4.

Figure 5 displays the measured X-band and Ka-band ETT carrier-to-noise signal levels (Pc/No) for each pass while the spacecraft was using a 61.5° telemetry modulation index at X-band along with predicted values (solid lines). Three-way peak signal strength data points are denoted by '3' and the one-way data points are denoted by '1' on this plot. Each X-band data point represents the averaged value of signal strength over each data set. Each Ka-band data point represents the peak value of signal strength fit over each data set which spans anywhere from a few minutes to several hours. For some of the tracks for which the Ka-band data displayed significant sinusoidal variations, this strategy removed much of the pointing error incurred over most of the pass due to the spacecraft spin (where the HGA boresight axis was misaligned with the spacecraft spin axis). Such variations in signal level of about 2 dB are consistent with expected values given the ~0.1° pointing knowledge of the spacecraft HGA (C. Chen 1996).

The predicted Pc/No values (solid lines in Figure 5) have been derived based on the following parameters and assumptions. The spacecraft EIRP used is 82.4 dBm for X-band three-way data, 82.0 dBm for X-band one-way data, and 76.0 dBm for all Ka-band data (C. Chen 1996). No correction has been applied in the predicted values for any possible spacecraft mis-pointing. The space-loss correction uses the range distances from navigation trajectory files. The carrier suppression correction due to ranging was about 0.2 dB for X-band

and 3.4 dB for Ka-band. The carrier suppression correction due to telemetry modulation assumed modulation indices of 61.5° for X-band and 63.6° for Ka-band. These modulation indices were estimated from carrier and data channel signal levels, Pc/No and Pd/No, acquired by DSS-13's advanced telemetry processor receivers (see 3c). The X-band value of 61.5° is consistent with an independent 61.2° value obtained from MGS X-band pre-flight measurements[1]. The thermal noise correction uses the Top data obtained from the TPR (see 3d). The atmospheric attenuation correction came from a model using input surface meteorological data. The ground station gain correction uses antenna efficiencies measured from experiments using natural calibrator radio sources (Morabito 1996).

Table 1 summarizes the statistics of the residual (measured minus predicted) Pc/No signal levels for each of the spacecraft modes (three-way and one-way), and telemetry modulation indices. Upon examining the Table 1 statistics and Figure 5, we find that the X-band Pc/No data are in agreement with the predicted values, ranging from 0 dB to -1.5 dB depending upon the spacecraft mode and modulation index.

Table 1
Residual (Observed - Predicted) Pc/No

Band	Mode	TLM Mod Index (Deg)	Average Pc/No Residual (dB)	Number of Passes	Number of Hours of Data
X	1-way	0	0.0	1	0.2
X	1-way	61.5	-1.33±0.48	15	35.4
X	3-way	61.5	-0.80±0.59	35	120.9
X	1-way	79.6	-1.45±1.01	4	7.5
X	3-way	79.6	0.00±0.38	57	232.4
Ka	1-way	0	-1.5	1	0.2
Ka	1-way	63.6	-6.34±2.10	15	20.6
Ka	3-way	63.6	-1.39±1.57	35	93.5
Ka	1-way	79.6 x 4	-6.00±2.81	4	6.9
Ka	3-way	79.6 x 4	-7.13±2.09	57	198.7

For the 63.6° telemetry modulation index three-way case (see Figure 5), the Ka-band data appear to agree best with the predicted values. This is especially evident for the three-way passes prior to the period of the suspected feedhorn crack (97-044 to 97-123) and after the "ICE FIX" on 97-206 (see 3a). The observed minus predicted Pc/No residual of -1.39±1.57 dB in Table 1 is the average value over all 35 passes for this case. These pass-to-pass statistics are consistent with 1 to 2 dB signal level variations expected from the ~0.1° pointing knowledge of the spacecraft HGA. For the 63.6° telemetry modulation index one-way case (see Figure 5 and Table 1), the Ka-band signal level data appear to be biased 5 dB below that of the three-way data. This bias is attributed to a reduced response of the spacecraft equipment at the higher Ka-band one-way frequency (32.008 GHz) relative to the lower three-way frequency (31.986 GHz).

For the 79.6° modulation index cases, the measured Ka-band signal levels lie significantly below the predicted values (see Table 1). These discrepancies are attributed to various effects of the flight hardware with the Ka-band signal due to 1) the higher 318° modulation index at Ka-band (79.6°x4), 2) the higher 320 kHz subcarrier frequency used at this modulation index (a lower 21.333 kHz subcarrier frequency is used during the 63.6° modulation index passes), 3) uncertainty in the carrier suppression correction due to modulation index uncertainty, and 4) the effect of spurious frequencies. In addition to this bias, the scatter in the observed values

[1] W. Adams, Private Communication, February 9, 1998

increase significantly after Mars orbit insertion (September 12, 1997 or 97-255) due to larger HGA pointing errors occurring during this period.

Figure 6 displays a projection of the Ka-band link advantage (vs X-band) and error bars using the 61.5°/63.6° telemetry modulation index data of Figure 5 normalized to equal conditions. The data from passes conducted during the period of accumulated ice inside the feedhorn (see 3a) were not included in Figure 6. This advantage is computed from the difference of the measured Ka-band and X-band Pc/No estimates which are corrected for preventable deficiencies at both bands; For equal spacecraft transmitted power, a 14-dB correction was applied (1 watt at Ka-band vs 25 watts at X-band). For expected future improved LNAs, the averaged Top over each pass was adjusted accordingly. The telemetry modulation and ranging channel carrier suppression contributions were backed out for both X-band and Ka-band. An additional correction was applied to the one-way data based on the measured difference between three-way and one-way data segments within a common pass. The result of Figure 6 confirms the predicted 5 dB Ka-band link advantage over X-band and by implication, minimized spacecraft antenna pointing loss for these passes which occurred during cruise before going into orbit around Mars.

4b) MGS Ka-band/X-band Solar Corona Experiment (May 1998)

Data were also acquired when MGS was angularly near the sun during the period around superior conjunction in May 1998. Because Ka-band signals are less affected by the Sun's corona than are X-band signals, Ka-band communications should be more easily maintained during solar conjunction. The projected advantage in Pc/No for Ka-band over X-band (see 4a) during the solar corona period is displayed in Figure 7. The observed increased Ka-band link advantage (Figure 7) over that observed during normal cruise (Figure 6) is apparent due to increased degradation of the X-band signal which in turn is attributed to the effects of spectral broadening and angular broadening. The significantly increased X-band noise temperature due to the solar corona and the wider ground antenna beamwidth significantly reduced the ETT detection threshold when the spacecraft was angularly near the sun. This, in turn, required loop bandwidth settings which were narrower than the broadened carrier signal spectrum at X-band.

4c) Frequency Data Analysis Results

This section reports on the X-band and Ka-band frequency data and frequency difference data acquired by the ETT at DSS-13. The data reported on here were acquired for passes conducted when the spacecraft Ka-band downlink frequency was coherent with the X-band downlink frequency. The ETT frequency data were processed using a Radio Science software package (Morabito and Asmar 1995) with trajectories generated by the MGS Navigation Team. The residuals for individual frequency band data were computed by removing a model frequency from each observable frequency at each time tag. The trajectory files were used to steer the frequency data into residuals for both X-band and Ka-band. A troposphere correction was applied to each data point.

Frequency residuals estimated for individual frequency bands are dominated by a combination of thermal noise, the USO (when in the one-way mode) and unmodeled dynamic spacecraft motion which appears in the form of significant systematic trends (sinusoidal signatures). These trends are believed to be due to dynamic motion of the spacecraft which is not modeled in the trajectory (spacecraft spin). The X-band and Ka-band Allan deviations were found to be in good agreement with each other for time intervals of τ = 1, 10, 100 and 1000 sec. The one-way data Allan deviations were also are in reasonable agreement with pre-flight values of the USO for all time scales except 1000 sec, where unmodeled spacecraft motion significantly contributes at higher time intervals.

For the passes where Ka-band is coherent with X-band, the received downlink Ka-band frequency is an exact factor of 3.8 times the X-band received frequency. By taking frequency differences across identical time tags of the form f_x-f_{Ka}/3.8, all non-dispersive error contributions, including unmodeled dynamic spacecraft motion, cancel out in the resulting difference residuals. The remaining noise sources should include thermal noise (significant at small time scales) and charged particles (which dominate at higher time scales). The

difference frequency residuals are effectively a measure of the charged particle effect on the X-band link since the effect at Ka-band is significantly smaller.

For all of the KaBLE-II passes conducted for which significant time periods of coherent X-band and Ka-band data were acquired, the Allan deviations of the difference data type (f_x-f_{Ka}/3.8) were estimated for time intervals of 1, 10, 100 and 1000 seconds. The Allan deviation for the shorter time intervals were generally in agreement with predictions based on thermal noise. The 1000-s Allan deviations are displayed in Figure 8 as a function of solar elongation angle. A general trend is apparent which shows Allan deviation decreasing as solar elongation angle increases from near 6° to about 170°. The expected thermal noise contributions to the 1000-s Allan deviations lie well below the observed Allan deviations. The observed 1000-s Allan deviations are consistent with expected solar plasma effects on the X-band link. The majority of the 1000-s Allan deviations clustered at high solar elongation angles in Figure 8 (above 160°) are in good agreement with a predicted Allan deviation value (6×10^{-15}) for the anti-solar direction at X-band (Armstrong, Woo and Estabrook, 1979).

5. CONCLUSION

The MGS/KaBLE-II link experiment measured signal strengths which were in general agreement with predicted values, and frequency residuals which were in agreement between bands and whose statistics were consistent with expected noise sources. The relative performance of X and Ka-band over an extended period will continue to be quantified as additional data are acquired under a wide range of elevation angles and atmospheric conditions. These efforts will continue with MGS/KaBLE-II as well as a future spacecraft with Ka-band and X-band signals, DS-1, which is scheduled for launch in October 1998.

ACKNOWLEDGMENTS:

We like to thank J. Border, R. Clauss, H. Cooper, C. Foster, A. del Castillo, P. Priest, M. Ryne, V. Vilnrotter, and J. Weese, all of JPL, and W. Adams and A. McMechen of Lockheed-Martin Astronautics Co. for their technical expertise and assistance; the DSS-13 station personnel for conducting the experiments (G. Bury, J. Crook, G. Farner, J. Garnica, R. Littlefair, R. Reese, L. Smith, L. Skjerve and L. Tanida); J. Caetta for software assistance; L. Teitelbaum and P. Wolken for scheduling support; and M. Speranza, T. Buckley and A. Milanian for assistance in data processing. This paper presents the results of one phase of research carried out at the Jet Propulsion Laboratory, California Institute of Technology, under contract with the National Aeronautics and Space Administration.

REFERENCES:

Armstrong, J. W., Woo, R. and Estabrook, F. B., "Interplanetary Phase Scintillation and the Search for Very Low frequency Gravitational Radiation", The Astrophysical Journal, 230, 570-574, June 1, 1979.

Butman, S. et. al. "The Mars Global Surveyor Ka-band Link Experiment (MGS/KaBLE-II)", in the proceedings of the 3rd Ka-band Utilization Conference, November. 1997, held in Sorrento, Italy.

Chen, C., "Mars Global Surveyor Project Telecommunications System operations Reference Handbook" , Version 2.1 542-257 (Internal JPL Document), September 1996.

Morabito, D.D., "The Efficiency Characterization of the DSS-13 34-Meter Beam-Waveguide Antenna at Ka-band (32.0 and 33.7 GHz) and X-band (8.4 GHz)", The Telecommunications and Data Acquisition Progress Report 42-125, vol. January - March 1996, Jet Propulsion Laboratory, Pasadena, California, May 15, 1996.

Morabito, D.D., and Asmar, S.W., "Radio Science Performance Analysis Software", The Telecommunications and Data Acquisition Progress Report 42-120, vol. October - December 1994, Jet Propulsion Laboratory, Pasadena, California, February 15, 1995, pp. 121-152.

Rebold, T. A., Kwok, A., Wood, G.D, and Butman, S. "The Mars Observer Ka-Band Link Experiment", The Telecommunications and Data Acquisition Progress Report 42-117, vol. January - March 1994, Jet Propulsion Laboratory, Pasadena, California, May 15, 1994.

Figure 1 - Pc/No for 97-212 Clear Weather Pass

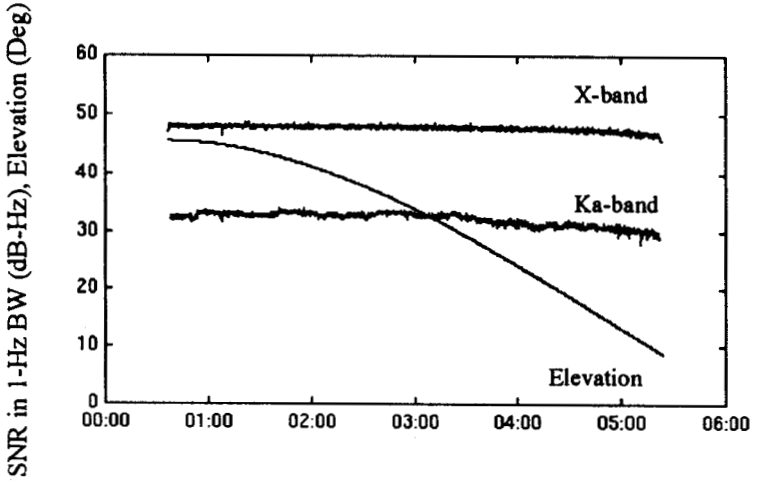

Figure 2 - Ka-band System Noise Temperature for 97-212

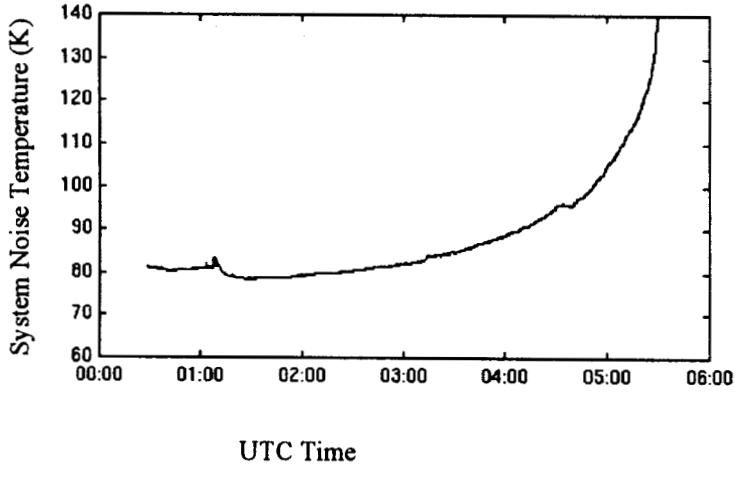

Figure 3 - Pc/No for 97-203 Rainy Weather Pass

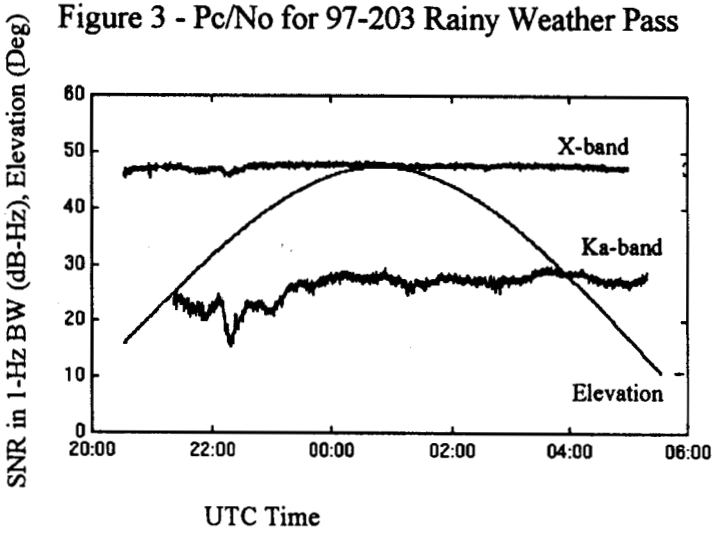

Figure 4 - Ka-band System Noise Temperature for 97-203

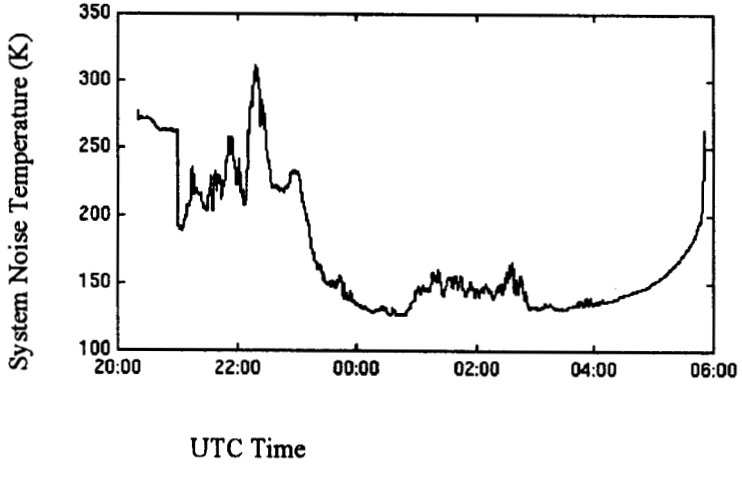

Figure 5 - Pc/No versus Day of Year

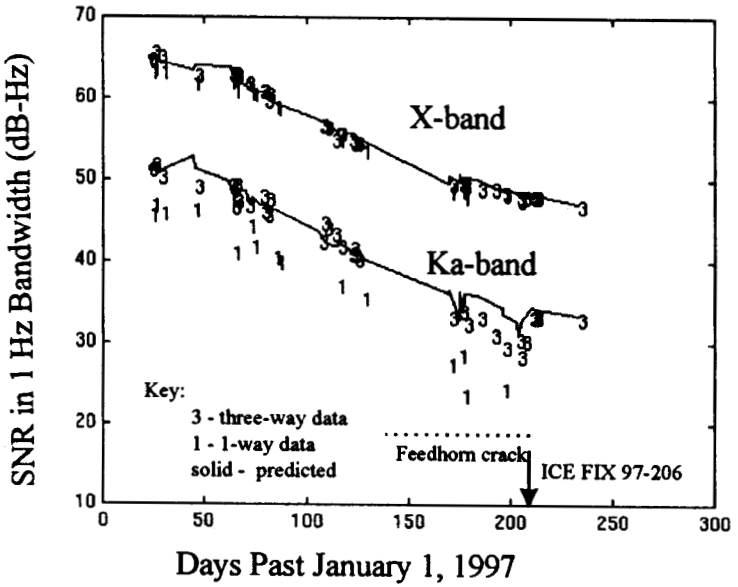

Figure 6 - Ka-band/X-band Link Advantage

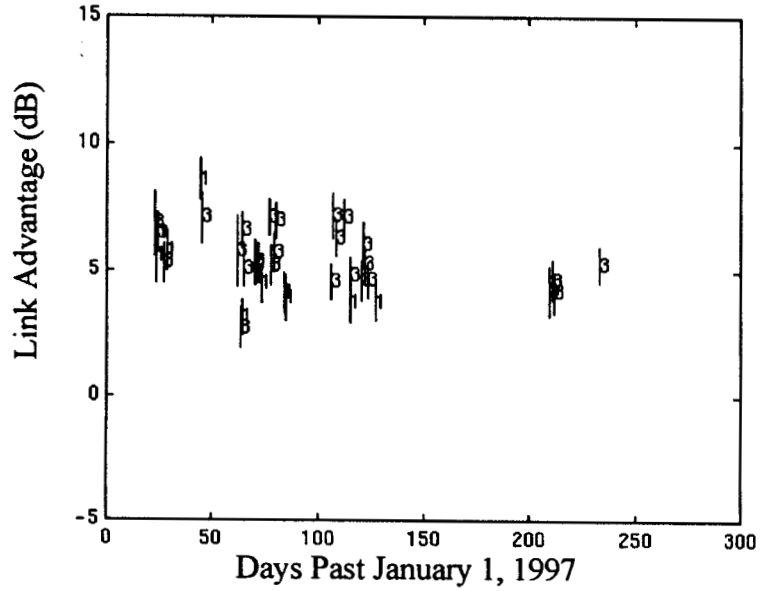

Figure 7 - Ka-band/X-band Link Advantage during Solar Conjunction May 1998

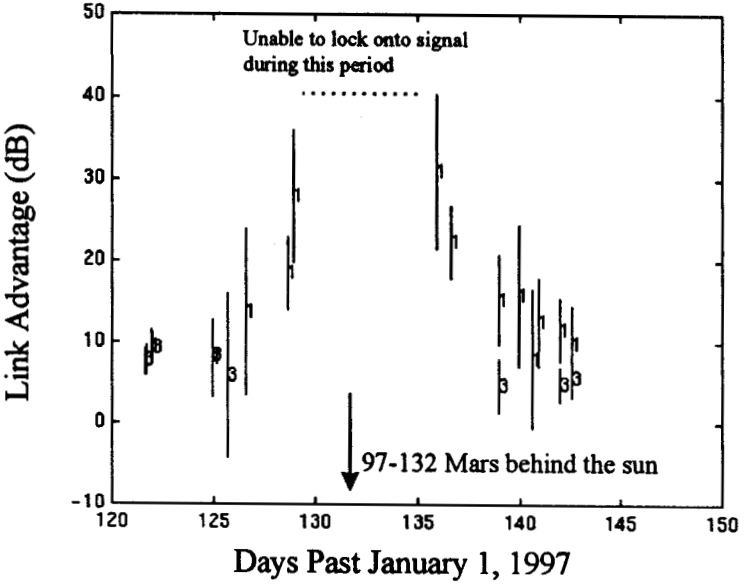

Figure 8 - f_x-f_{Ka}/3.8 Allan Deviation at 1000 seconds